Surface & Coatings Technology xxx (xxxx) xxx–xxx

Contents lists available at ScienceDirect

Surface & Coatings Technology

journal homepage: www.elsevier.com/locate/surfcoat

Structural and optoelectrical properties of Nb-TiO_2 films fabricated by low-energy magnetron sputtering and post-annealing☆

Cuiqing Jiang[a], Zhongzhen Wu[a,b,*], Shu Xiao[a], Zhengyong Ma[a], Liangliang Liu[a], Ricky K.Y. Fu[b], Paul K. Chu[b], Hai Lin[a], Feng Pan[a]

[a] School of Advanced Materials, Peking University Shenzhen Graduate School, Shenzhen 518055, China
[b] Department of Physics and Materials Science, City University of Hong Kong, Tat Chee Avenue, Kowloon, Hong Kong, China

A R T I C L E I N F O

Keywords:
NTO
Film thickness
Electrical conductivity
Optical transmittance

A B S T R A C T

Nb-doped TiO_2 (NTO) films have potential to replace indium tin oxide (ITO) as transparent conducting material. However, costly substrates with a specific orientation such as sapphire must be used to avoid formation of the rutile phase and to obtain transparent and conductive NTO films. Furthermore, scaling up is difficult thus hampering commercialization. Herein, in order to control the crystal orientation of TiO_2, two-step preparation is described. An amorphous NTO film is first prepared on the economical soda-lime glass substrate by low-energy magnetron sputtering and the sample is annealed in Ar with 5 at% H_2 at 400 °C to crystallize the amorphous structure into anatase (101) and anatase (004). The morphology, structure, and optoelectrical properties of the NTO films and relationship with film thickness are studied. The resistivity decreases to 8.1×10^{-4} Ω·cm for a thickness of 320 nm and the average transmittance in the visible region increases monotonically to 73% as the thickness is reduced from 400 nm to 280 nm. The good conductivity and transmittance suggest potential application to smart windows and solar cells.

1. Introduction

Transparent conductive oxides (TCOs) are widely used as transparent electrodes in optoelectronic devices such as flat-panel displays [1], solar cells [2], smart windows and light-emitting diodes [3, 4]. Sn-doped In_2O_3 (ITO) is the most extensively used TCO due to its low resistivity (2–3 × 10^{-4} Ω·cm) and high transparency in the visible region (80%–90%) [5–7]. However, shortage of indium as demands ramp up is a big concern and hence, alternative TCO materials composed of more abundant and nontoxic elements have aroused interest [8]. Nb-doped TiO_2 (NTO) is attractive due to the high conductivity and transparent properties [9]. Recently, NTO films prepared by pulsed laser deposition (PLD) [10], sputter deposition, and the sol-gel method [11–13] have been reported. Furubayashi et al. [10] found that pure anatase NTO epitaxial films prepared on single-crystal $SrTiO_3$ (100) substrates by PLD exhibited small resistivity of 3×10^{-4} Ω·cm and excellent transmittance of > 90% in the visible region. However, a substrate with a specific orientation such as $SrTiO_3$ (100) must be used to avoid formation of the rutile phase and so large-scale production is difficult. Furthermore, when a glass substrate is used to deposit conductive NTO films by PLD, a resistivity on the order of 10^{-4} Ω·cm can be obtained under the optimal conditions but the transmittance is only ~60% [12], which is not good enough for many applications. Sputtering has also been used to deposit NTO films on a large substrate with high throughput [13] and in order to avoid forming the rutile phase and improve the transparent property, a two-step process in which an amorphous NTO films is fabricated by magnetron sputtering and then crystallization occurs during annealing in H_2, vacuum, or N_2 [14]. However, the compromise between conductivity and transmittance is not well understood [15, 16]. It has been shown that the thickness of the NTO films (mostly < 200 nm for high transmittance) is positively related to the conductivity [17] but thicker TCO films are required in some applications such as CIGS and CdTe thin-film solar cells [18–20].

In this work, NTO films with different thicknesses are fabricated on the soda-lime glass substrate by a two-step process including low-energy magnetron sputtering and post-annealing in order to restrain the formation of poor optoelectrical rutile. The relationship between the structural, morphological, optical and electrical properties and film thickness is investigated in order to improve both the electrical conductivity and optical transparency.

☆ The 14th International Conference on Plasma Based Ion Implantation & Deposition.

* Correspondence to: Z. Wu, School of Advanced Materials, Peking University Shenzhen Graduate School, Shenzhen 518055, China.
E-mail address: wuzz@pkusz.edu.cn (Z. Wu).

https://doi.org/10.1016/j.surfcoat.2018.05.092
Received 4 January 2018; Received in revised form 3 May 2018; Accepted 22 May 2018
0257-8972/ © 2018 Elsevier B.V. All rights reserved.

Please cite this article as: Jiang, C., Surface & Coatings Technology (2018), https://doi.org/10.1016/j.surfcoat.2018.05.092

2. Experimental details

The NTO films were prepared in a vacuum chamber with a diameter of 60 cm and height of 50 cm. Before loading into the chamber, the soda-lime glass substrates were ultrasonically cleaned in ethanol and acetone for 30 min at room temperature (RT). A NTO target (95 at% TiO_2 and 5 at% Nb) 60 mm in diameter and 6 mm thick was mounted in the magnetron sputtering source. The soda-lime glass substrates were placed at a distance of 18 cm from the NTO target. After the chamber was evacuated to a base pressure of 8×10^{-4} Pa, the Ar gas (99.99% pure) flow rate was maintained at 8 sccm to keep the working pressure at 0.3 Pa. The NTO films were deposited on the substrates by direct-current magnetron sputtering (DCMS) at a current of 0.1 A and voltage of 370 V. The thickness of the NTO films was controlled by the sputtering time. After deposition, the samples underwent two-step annealing in Ar gas with 5 at% H_2. In the first step, the annealing temperature rose from room temperature to 250 °C at a heating rate of 10 °C per minute and the temperature was maintained for 0.5 h. In the second step, the annealing temperature was raised to 400 °C using the same heating rate and kept for 2 h. The samples were cooled inside the furnace to room temperature.

The crystalline structure was determined by X-ray diffraction (XRD, Bruker D8 Advance) in the continuous scanning mode using Cu K_α radiation. The coating thickness was measured by scanning electron microscopy (SEM, ZEISS SUPRA® 55). The electrical properties were characterized on a Hall Effect System (Ecopia, HMS3000) and the chemical composition determined by X-ray photoelectron spectroscopy (XPS, ESCALAB 250X, Thermo Fisher, UK). The binding energy was referenced to the C1s peak at 284.6 eV. The transmittance and absorption properties were determined by ultraviolet-visible (UV–vis) spectrophotometry (Shimadzu, UV-2450) using a soda-lime glass substrate as a reference and the average transmittance in the visible region (400–760 nm) was calculated.

3. Result and discussion

Fig. 1 shows the cross-sectional SEM images revealing that the thicknesses of the NTO films are 280 nm, 320 nm, 360 nm, and 400 nm as the sputtering time is increased from 140 min to 200 min with a depositing rate of 2 nm/min. The cross- sectional SEM images of all samples show flat structure without appearance of obvious grain boundaries indicating some amorphous structures may be created by the low-energy deposition at a small sputtering current [21]. No apparent defects can be observed at the interfaces. The adhesion strength between the NTO films and glass substrates are measured by the adhesion cross cut test with a case size of 1 × 1 mm and shown in the inserts. All the peeling-off areas are below 5% of the total areas revealing excellent adhesion (Level 4B, ASTM D3359).

Fig. 2 shows the structural evolution of the NTO films before and after post-annealing monitored by XRD. No apparent peaks can be observed from the films indicating an amorphous structure consistent with SEM as shown in Fig. 2(a). After post-annealing, the NTO films crystallize and two obvious peaks at 25.6° and 38.2° corresponding to the anatase (101) and anatase (004) orientations, respectively, emerge, as shown in Fig. 2b. The intensity of the anatase (101) peak is almost constant while that of anatase (004) increases with thickness up to 320 nm. The largest intensity is observed when the thickness is 320 nm, indicating good crystallization. Although the rutile (210) peak at 44.8° and rutile (211) peak at 54.3° are observed from all samples after annealing at 400 °C [22, 23], the peak intensity is quite low. All in all, the results show that the anatase NTO films can be produced on a glass substrate by the two-step process involving low-energy magnetron sputtering and post-annealing.

TEMs of the different samples are performed and the results are shown in Fig. 3. The grains with the two preferred orientations, anatase (101) and (004), are marked by yellow and red lines, respectively. The results reveal that the grain sizes are about 5–20 nm and are declining with the decreasing thickness. This phenomenon is consist with many previous reports and demonstrated by the effect of grain grooves (the thermal pitting of a surface in the vicinity of a grain boundary vertex) on grain size [24–29].

The surface composition and chemical states are determined by XPS and the results are shown in Fig. 4. Nb, Ti and O are detected as shown in Table 1. With the increase of the NTO thickness, the Nb and O concentrations increase from 2.56 at% to 2.74 at% and from 61.13 at% to 61.76 at%, respectively, whereas the Ti concentration decrease from 36.31 at% to 35.51 at%. The composition variation of Nb and Ti may be influenced by sputtering threshold energy and deposition temperature increase with the film thickness [30, 31]. The Nb peak in Fig. 4(a) is composed of two peaks at binding energies of 207 eV and 204 eV corresponding to Nb^{5+} and Nb^{2+}, respectively. The results suggest successful Nb incorporation into the TiO_2 lattice as a result of the larger electronegativity of Nb (1.60) than that of Ti (1.54) [32], large amount of oxygen vacancy, and reductive Nb^{2+} produced during annealing in the oxygen-free atmosphere.

Fig. 5 shows the Hall measurement results of the NTO films for different thicknesses. The resistivity of NTO films is related to the carrier concentration and Hall mobility. The carrier concentration increases from 1.0×10^{21} cm^{-3} to 1.4×10^{21} cm^{-3} monotonically with thickness, which is closely related to Nb content. The Hall mobility increases from 4.8 cm^2/Vs to 7.4 cm^2/Vs initially due to the increase of grain size and Nb content [14, 32] but decreases when the film thickness is larger than 320 nm. The decrease of Hall mobility is mainly because of the increasing combination of electrons and holes accompanying with the increasing of oxygen vacancies [33–35]. Due to the high Hall mobility, the smallest resistivity of 8.1×10^{-4} Ω·cm is achieved for the 320 nm thick NTO film.

The optical transmittance performance of the NTO films is important. Fig. 6 shows the optical transmittance and absorption in the visible range (320–780 nm) of the NTO films with different thicknesses and the average values are given in the insets. Although these NTO films are thicker than those reported before, the optical transmittance is still very large and the average transmittance in the visible region (400–760 nm) increases from 66.2% to 73.2% as the thickness decreases from 400 nm to 280 nm. Considering both the electrical and optical properties, the NTO film with a thickness of 320 nm has the best TCO characteristics. Obviously, the thickness increases the path for light absorption reducing the transmittance [17]. Besides, the anatase-dominated orientation in the NTO films results in good conductivity and transmittance [23]. The optical absorption of the NTO films show an opposite evolution with film thicknesses, but the largest average absorption in the visible region (400–760 nm) is only 0.19% when the film thickness is 400 nm. It has been shown that the reflection contributes to loss of transmittance because of the large difference in the refractive indexes between NTO and air [23, 36].

4. Conclusion

NTO films are fabricated on a soda-lime glass substrate by a two-step process involving low-energy magnetron sputtering and post-annealing. The anatase (101) and (004) polycrystalline NTO films are obtained and the morphology, composition, as well as optical and electrical properties are determined from films with different thicknesses. Owing to the larger grain size and Nb content in a thicker film, the carrier concentration and Hall mobility increase initially but the Hall mobility decreases as a result of the increasing combination of electrons and holes accompanying with the increasing of oxygen vacancies. The smallest resistance of 8.1×10^{-4} Ω·cm is achieved from the film with a thickness of 320 nm. Although the dominant anatase phase improves the transmittance in the visible range significantly, the best average transmittance is 73% due to reflection. Nonetheless, our results indicate that the polycrystalline anatase-dominant NTO films

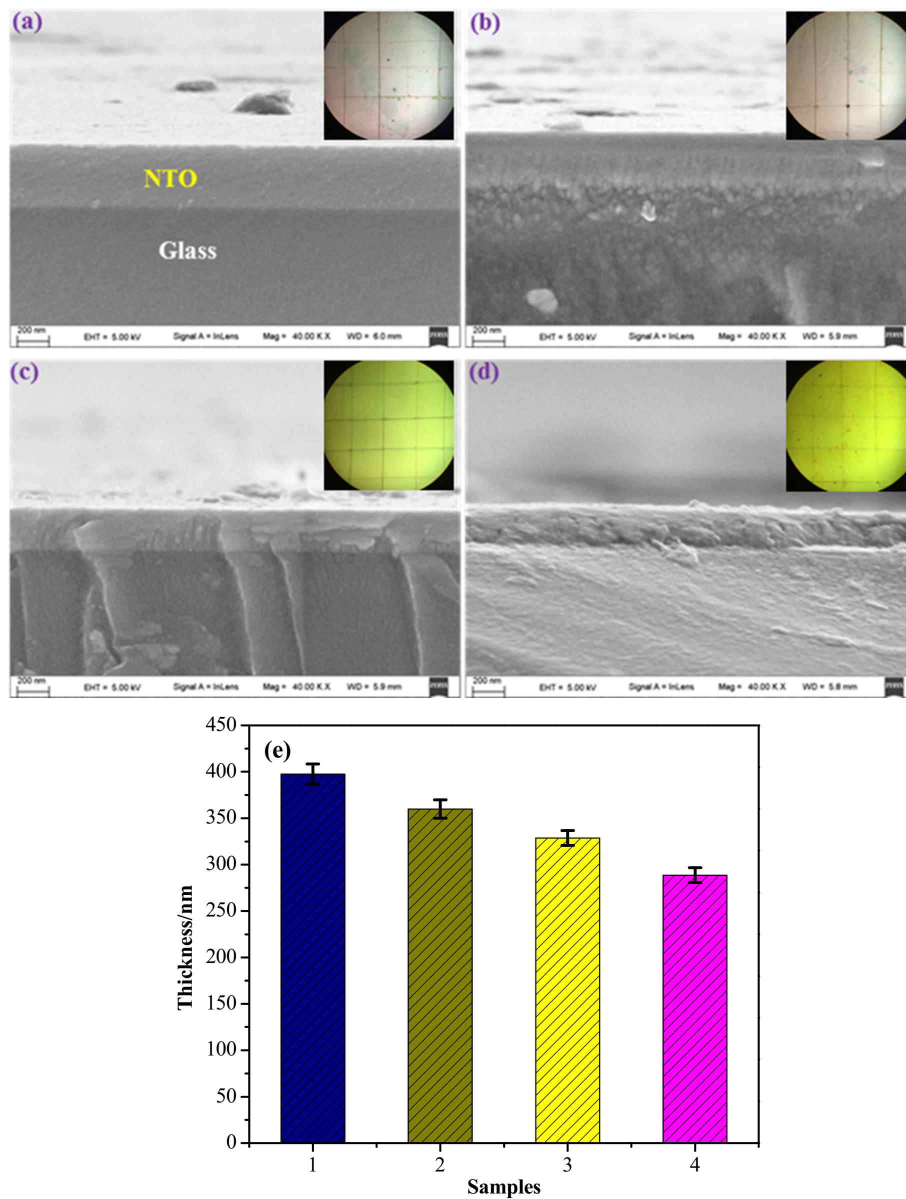

Fig. 1. Cross-sectional SEM images and the surface morphologies after cross cut test of the as-deposited NTO films deposited for (a) 200 min, (b) 180 min, (c) 160 min, and (d) 140 min; (e) film thickness.

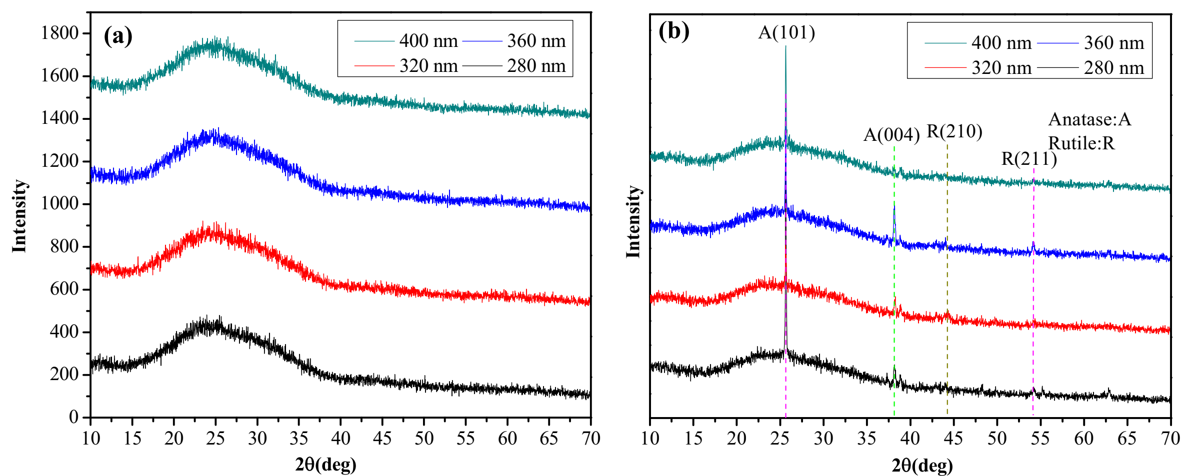

Fig. 2. XRD patterns of the NTO films produced on the glass substrate: (a) As-deposited and (b) annealed.

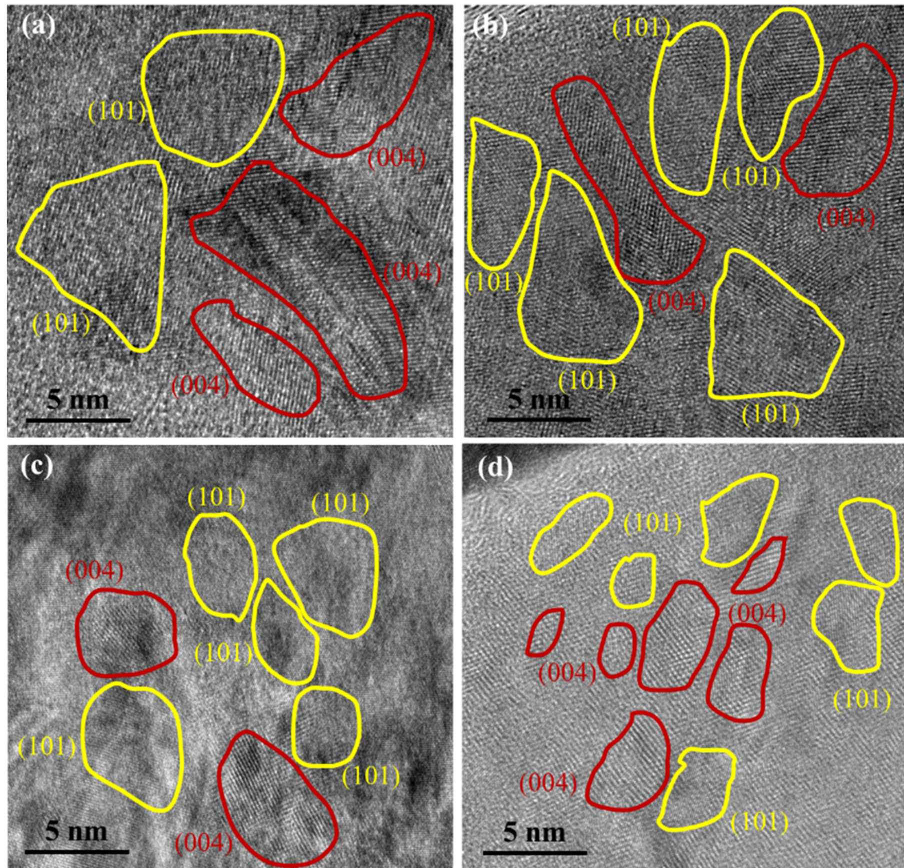

Fig. 3. TEM images of NTO film after annealed: (a) 400 nm; (b) 360 nm; (c) 320 nm; (d) 280 nm.

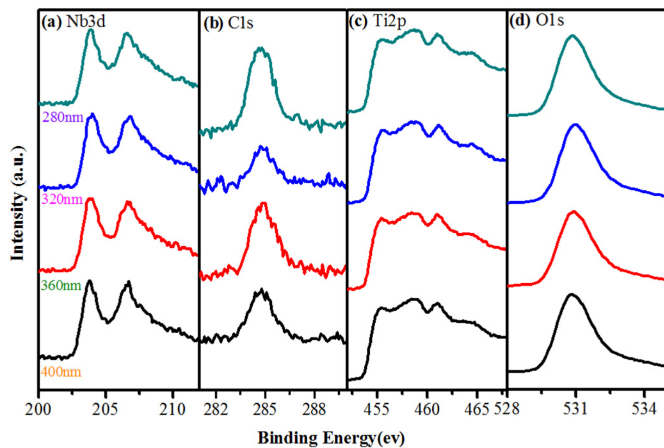

Fig. 4. XPS spectra of the NTO films with different thicknesses: (a) Nb 3d, (b) C1s, (c) Ti 2p, and (d) O 1s.

Table 1
Composition (at%) of the NTO films with different thicknesses after post-annealing.

Samples	400 nm	360 nm	320 nm	280 nm
Nb	2.74	2.72	2.68	2.56
Ti	35.51	35.68	36.04	36.31
O	61.76	61.60	61.28	61.13

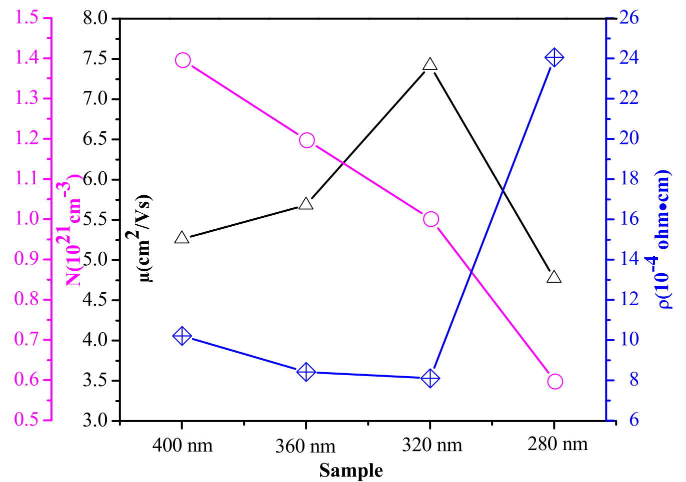

Fig. 5. Hall mobility (μ), carrier concentration (N), and resistivity (ρ) of the NTO films with different thicknesses.

have large potential as TCO materials but introduction of an antireflective film may be needed for further improvement.

Acknowledgements

This work was financially supported by National Materials Genome Project (No. 2016YFB0700600), Guangdong Applied Technology Research Special Project (Grant No. 2015B090927003), Shenzhen Science and Technology Research Grants (JCYJ20150828093127698 and GJHS20170313150213648), as well as City University of Hong Kong Applied Research Grant (ARG) No. 9667122 and Strategic

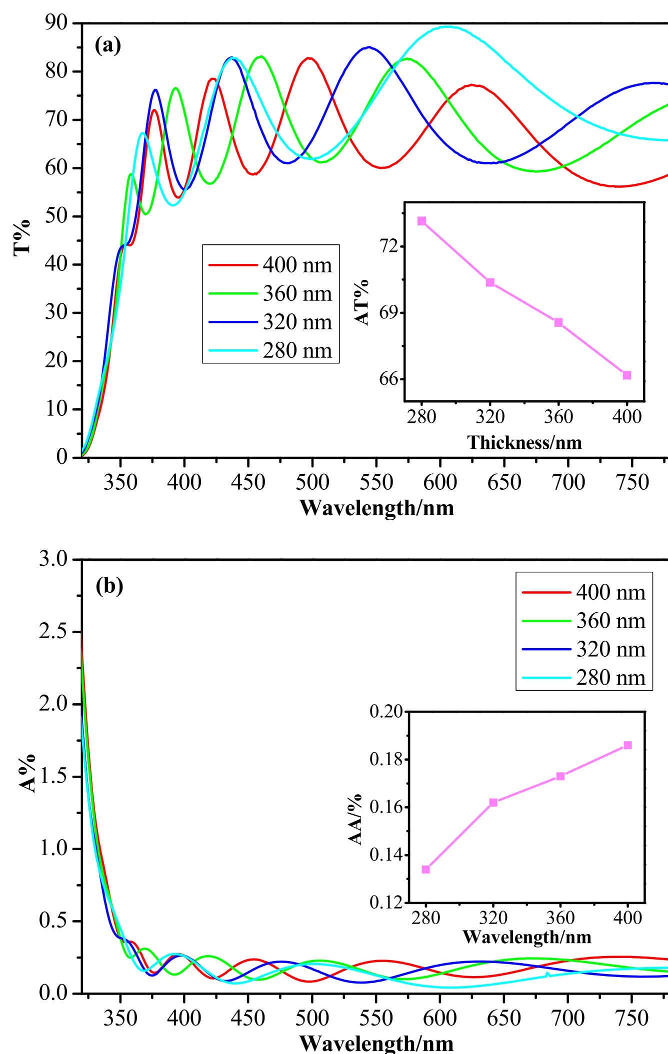

Fig. 6. (a) Optical transmittance and (b) optical absorption as a function of wavelength in the range of 320–780 nm obtained from the NTO films with different thicknesses. The insets in (a) and (b) show the average transmittance and average absorption in the visible region (400–760 nm).

Research Grant (SRG) No. 7004644.

References

[1] J.T. Michael, M. Lee, Tsutomu Miyasaka, Takurou N. Murakami, Henry J. Snaith, Science 338 (2012) 643–647.
[2] J.F. Wager, Science 300 (2003) 1245–1246.
[3] V. Bulović, P. Tian, P.E. Burrows, M.R. Gokhale, S.R. Forrest, M.E. Thompson, Appl. Phys. Lett. 70 (1997) 2954.
[4] G.J. Exarhos, X.D. Zhou, Thin Solid Films 515 (2007) 7025–7052.
[5] G.K.R. Senadeera, K. Nakamura, T. Kitamura, Y. Wada, Appl. Phys. Lett. 83 (2003) 5470–5472.
[6] K.L. Chopra, S. Major, D.K. Pandya, Thin Solid Films 102 (1983) 1–46.
[7] M. Tzolov, N. Tzenov, D. Dimova-Malinovska, M. Kalitzova, C. Pizzuto, G. Vitali, G. Zollo, I. Ivanov, Thin Solid Films 379 (2000) 28–36.
[8] E.M. Kaidashev, M. Lorenz, H. Von Wenckstern, A. Rahm, Appl. Phys. Lett. 82 (2003) 3901–3903.
[9] X. Yang, M.J. Zhang, Y. Min, M. Xu, Z. Mei, J. Liang, J. Hu, S. Yuan, S. Xiao, Y. Duan, F. Liu, H. Lin, Y. Lin, F. Pan, ACS Appl. Mater. Interfaces 9 (2017) 29021–29029.
[10] Y. Furubayashi, T. Hitosugi, Y. Yamamoto, K. Inaba, G. Kinoda, Y. Hirose, T. Shimada, T. Hasegawa, Appl. Phys. Lett. 86 (2005).
[11] Y. Furubayashi, T. Hitosugi, Y. Yamamoto, Y. Hirose, G. Kinoda, K. Inaba, T. Shimada, T. Hasegawa, Thin Solid Films 496 (2006) 157–159.
[12] K. Tonooka, T.W. Chiu, N. Kikuchi, Appl. Surf. Sci. 255 (2009) 9695–9698.
[13] G. Wan, S. Wang, X. Zhang, M. Huang, Y. Zhang, W. Duan, L. Yi, Appl. Surf. Sci. 357 (2015) 622–625.
[14] L. Zhang, X. Xiao, X. Zhou, H. He, X. Xu, Q. Lin, H. Zhou, S. Zhang, H. Zhang, Q. Liu, J. Vac. Sci. Technol. A 34 (2016) 051512.
[15] L. Zhao, X. Zhao, J. Liu, A. Zhang, D. Wang, B. Wei, J. Sol-Gel, Sci. Technol. 53 (2010) 475.
[16] C. Wang, J. Meinhardt, P. Löbmann, J. Sol-Gel Sci. Technol. 53 (2010) 148–153.
[17] Z.L. Tseng, L.C. Chen, J.F. Tang, M.F. Shih, S.Y. Chu, J. Electron. Mater. 46 (2016) 1476–1480.
[18] M.E.S.E.R. Ollotu, R.T. Kivaisi, Int. J. Nano Sci. Technol. 2 (2014) 1–10.
[19] X. Lü, X. Mou, J. Wu, D. Zhang, L. Zhang, F. Huang, F. Xu, S. Huang, Adv. Funct. Mater. 20 (2010) 509–515.
[20] J. Kasai, T. Hitosugi, M. Moriyama, K. Goshonoo, N.L.H. Hoang, S. Nakao, N. Yamada, T. Hasegawa, J. Appl. Phys. 107 (2010).
[21] N. Yamada, T. Hitosugi, N.L.H. Hoang, Y. Furubayashi, Y. Hirose, T. Shimada, T. Hasegawa, Jpn. J. Appl. Phys. 46 (2007) 5275–5277.
[22] N.L. Huong Hoang, N. Yamada, T. Hitosugi, J. Kasai, S. Nakao, T. Shimada, T. Hasegawa, Appl. Phys. Express 1 (2008) 115001–115003.
[23] N. Yamada, T. Hitosugi, N.L.H. Hoang, Y. Furubayashi, Y. Hirose, S. Konuma, T. Shimada, T. Hasegawa, Thin Solid Films 516 (2008) 5754–5757.
[24] A. Novick Cohen, O. Zelekman-Smirin, A. Vilenkin, Acta Mater. 58 (2010) 813–822.
[25] W.W. Mullins, Acta Metall. 6 (1957) 414–427.
[26] A.J. Dammers, S. Radelaar, Textures Microstruct. 14 (1991) 757–762.
[27] J.M. Thijssen, Phys. Rev. B Condens. Matter 51 (1995) 1985.
[28] J.H. Kim, T.Y. Seong, K.J. Ahn, K.B. Chung, H.J. Seok, H.J. Seo, H.K. Kim, Appl. Surf. Sci. 440 (2018).
[29] N. Arshi, L.U. Junqing, G.L. Chan, J.H. Yoon, B.H. Koo, F. Ahmed, Bull. Mater. Sci. 36 (2013) 807–812.
[30] D.E. Harrison Jr., G.D. Magnuson, Phys. Rev. 122 (1961) 1421–1430.
[31] C. Garciá-Rosales, J. László, W. Eckstein, J. Roth, Nucl. Instrum. Methods Phys. Res. 83 (1993) 95–109.
[32] H. Su, Y.T. Huang, Y.H. Chang, P. Zhai, N.Y. Hau, P.C.H. Cheung, W.T. Yeh, T.C. Wei, S.P. Feng, Electrochim. Acta 182 (2015) 230–237.
[33] L. Sagalowicz, G.R. Fox, J. Mater. Res. 14 (1999) 1876–1885.
[34] K. Nomura, H. Ohta, A. Takagi, T. Kamiya, M. Hirano, H. Hosono, Nature 432 (2004) 488–492.
[35] R. Asahi, Y. Taga, W. Mannstadt, A.J. Freeman, Phys. Rev. B Condens. Matter 61 (2000) 7459–7465.
[36] G.E. Jellison Jr., L.A. Boatner, J.D. Budai, B.S. Jeong, D.P. Norton, J. Appl. Phys. 93 (2003) 9537–9541.